



# Membrane crystallinity and fuel crossover in direct ethanol fuel cells with Nafion composite membranes containing phosphotungstic acid

Hongjun Kim<sup>1</sup>, Sunghwan Lee<sup>2,\*</sup>, Suran Kim<sup>1</sup>, Chungik Oh<sup>1</sup>, Jeongjae Ryu<sup>1</sup>, Jaegyung Kim<sup>1</sup>, Eugene Park<sup>4</sup>, Seungbum Hong<sup>1,3</sup>, and Kwangsoo No<sup>1,\*</sup>

<sup>1</sup>Department of Materials Science and Engineering, KAIST, Daejeon 305-701, South Korea

<sup>2</sup>Department of Mechanical Engineering, Baylor University, Waco, TX 76798, USA

<sup>3</sup>Materials Science Division, Argonne National Laboratory, Lemont, IL 60439, USA

<sup>4</sup>Materials and Energy Science and Engineering, Nelson Mandela African Institute of Science and Technology, Arusha, Tanzania

Received: 10 July 2016

Accepted: 24 October 2016

Published online:

1 November 2016

© Springer Science+Business Media New York 2016

## ABSTRACT

We report on the effect of the addition of phosphotungstic acid (PWA) in Nafion membrane on ethanol-crossover and the proton conductivity for DEFC application. A set of PWA–Nafion composite membranes (PWA 0, 5, 10, 15, 20 wt%) was prepared by solution casting and their microstructures, diffraction patterns, permeability, and proton conductivity were systematically characterized. The significant reduction in ethanol-crossover is observed with increasing PWA concentration in PWA–Nafion membranes, which is mainly attributed to an improvement in crystallinity of the membrane. PWA provides additional nucleation sites during solidification leading to higher crystallinity, which is supported by the membrane permeability tests. The proton conductivity of the composites is enhanced with PWA concentration until 15 wt% due to an increase in hopping pathways, while higher PWA of 20 wt% leads to a conductivity decrease possibly due to the excessive particle aggregations that limit ion transports. These PWA–Nafion composites were implemented in prototype DEFC devices as a membrane and the maximum power density achieved was 22% higher than that of commercial Nafion-117 device.

## Introduction

In recent years, interest in portable electronic devices, such as cell phones and laptop computers, has been rapidly growing and, therefore, various energy storage and conversion systems have emerged in order to

provide electrical power for portable devices with mechanical stability and high efficiency as well as environmental benefit and cost-effectiveness [1]. Proton exchange membrane fuel cells (PEMFCs), typically employing hydrogen gas as a fuel, have been extensively investigated as a result of the well-

Address correspondence to E-mails: sunghwan\_lee@baylor.edu; ksno@kaist.ac.kr

known properties of high energy density ( $\sim 2000$  kW/L), high power conversion efficiency (50–55%), low operating temperatures (60–80 °C) [2], short startup times, and low emission of pollutants [3]. However, the practical application of PEMFC is challenging due to the complexity of storing and delivering hydrogen gas. Efforts [4–8] to integrate other fuels to replace  $H_2$  have been made. Direct alcohol fuel cells (DAFCs) that use liquid phase fuels (i.e., alcohol) are garnering much attention for portable device application due mainly to the convenience of carrying liquid fuels compared to the use of the unsafe gas phase  $H_2$  fuel. Among several types of DAFCs, methanol and ethanol are generally considered as a fuel: methanol-DAFCs (DMFCs) have been reported to show 35–50% electrical density for Nafion electrolyte, while ethanol-DAFCs (i.e., direct ethanol fuel cells, DEFCs) present 20–40% electrical density for the same Nafion membrane system [2]. While the performance of DMFCs is slightly higher than that of DEFCs, the implementation of methanol for fuel cell application is limited due to its toxicity [9]. Therefore, interest has been growing in DEFCs due to the properties of ethanol which are non-toxicity, high energy density, low cost, and potential contribution to energy issues in third world countries [10].

The relatively low power conversion efficiency of DEFCs is primarily attributed to the ethanol-crossover [11], which generally describes that the ethanol fuel penetrates through the electrolyte membrane and moves toward the other electrode (i.e., cathode) during fuel cell operation. This ethanol-crossover significantly reduces the output voltages and, consequently, results in low device performance. Previous reports [12–14] to improve the ethanol-crossover and to enhance DEFC performance are available in the literature: Barbara et al. [12] reported that Nafion-titania composite membrane reduced the ethanol-crossover. They revealed that the increased crystalline domains of the composite membrane result in a decrease in fuel permeability, as crystalline surfaces are known to be less permeable to liquid phases compared to amorphous surfaces. Furthermore, the proton conductivity also increased because the strong oxidation potential of titania led to the formation of additional OH groups on the surface of the particles. These OH groups increase the number of ion exchange sites which facilitate the transport of protons [12]. Battirolo et al. [13] proposed the doped Nafion electrolyte membranes in which platinum (Pt)

and platinum–ruthenium (Pt–Ru) nanoparticles were used to improve ethanol-crossover in DEFC application. The extra catalytic sites generated by the addition of nanoparticles oxidize residual ethanol, thus preventing ethanol-crossover [13]. Maab and Nunes demonstrated [14] membranes for DEFCs made of sulfonated poly(ether ether ketone) (SPEEK) coated with carbon molecular sieves (CMSs). The nanoporous structure of the CMSs reduces alcohol crossover during fuel cell operation and SPEEK blended with hydrophobic polyimide further improves alcohol crossover due to its hydrophobic nature. Although the proton conductivity of the SPEEK–polyimide composites is relatively lower than Nafion membranes; a higher DEFC performance at 90 °C was achieved compared to those using Nafion membranes due mainly to the effective reduction of ethanol-crossover [14].

Heteropolyacids (HPAs), such as PWA, are well known as superionic conductors in their fully hydrated states [15, 16]. The main interesting properties of HPAs include their strong acidity and the structure. As pure Brønsted acids, the solid-state HPAs show higher acidity than the conventional solid acids such as  $SiO_2$ ,  $Al_2O_3$ , and zeolites. The Keggin structure, which is the typical local structure of HPAs, is identified as a general formula of  $[H_3XM_{12}O_{40}]$ , where X is the central atom (e.g., Si, P) tetrahedrally linked to oxygen and surrounded by the oxygen-linked peripheral metal atom, M (e.g., Mo, W, V, Co), or a combination of metals [17]. The dispersion of the negative charge over many oxygen atoms of the polyanion  $[XM_{12}O_{40}]^{3-}$  and the oxygen–metal double bond, which polarizes the negative charge of oxygen to M that limits distribution of the negative charge in the outer surface of the polyanion [18], are the two determining factors of HPA acidity. Additionally, their strong acidity is known to lead to an increase in proton conductivity, which is favorable in DAFC application [18]. Due to the intrinsic proton conductivity of HPAs and good chemical compatibility with other polymers, HPAs have been used to synthesize composites with various polymer matrices including Nafions, polybenzimidazole, and poly(ether ether ketone) (known as PEEK) [19–22].

Among the Keggin-type HPAs, PWA ( $H_3PW_{12}O_{40}$ ) shows the highest conductivity and strongest acidity [23, 24]. Amirinejad et al. [17] prepared nanocomposite Nafion membranes which consist of PWA with cesium ions by recast procedure, and the PEMFC

performance was evaluated at a high temperature (110 °C) and the results showed that the PWA particles improved water retention ability, thermal stability, and proton conductivity of Nafion. Particularly, they suggest that the hydrophilic nature of PWA particles prevents from the evaporation of the water molecules and subsequently increases the ability to retain water molecules, which results in the higher PEMFC performance. Malhotra and Datta [25] proposed PWA-impregnated Nafion membrane, processed using PWA solution with various solvents (e.g., acetic acid and tetra-*n*-butylammonium chloride) and demonstrated improved PEMFC performance. They reported that the added PWA acid increased the proton density in pores in the membrane, similarly as water does in conventional Nafion membrane. Lu et al. [26] developed a multilayer membrane that consists of mesoporous Nafion, which was fabricated using a soft-templating method with a non-ionic block copolymer. The mesoporous Nafion was impregnated with PWA and sandwiched between Nafion membranes. The multilayer membrane exhibited much higher conductivity and device performance due to the higher water retention ability of PWA than that of pristine Nafion. Abouzari-Iotf et al. [27] reported on the incorporation of electrospun nylon-66 nanofibrous sheets with dispersed PWA in the tri-layer Nafion-based membranes to improve the methanol barrier property of Nafion in PEMFC and DMFC [28] application. The addition of nylon-66 nanofibrous sheet covered with PWA particles showed a positive effect to enhance proton conductivity due to provision of proton transfer path by PWA particles on the fibrous structure. Xiang et al. [23] also reported that the addition of phosphotungstic acid (PWA) in Nafion membrane was of important use to suppress methanol-crossover without any significant degradation in proton conductivity for DMFC application. They attributed this improvement to a decrease in the size of hydrophilic water-rich domain, through which methanol permeates, while maintaining the proton conductivity by virtue of the high ionic conductive nature of PWA.

Although many studies have focused on the incorporation of PWA in electrolyte membranes for low-temperature fuel cells, such as PEMFCs [17, 29] and DMFCs [24, 30], the effect of PWA addition in membrane for more environmentally friendly and non-toxic DEFCs has been rarely investigated. In this study, PWA–Nafion composite membranes were

synthesized as a function of PWA concentration and were implemented in direct ethanol fuel cells in order to investigate the effect of PWA on the ethanol-crossover as well as proton conductivity in DEFC performance. The PWA–Nafion composites were systematically characterized using X-ray diffraction to determine amorphous/crystalline structure, and scanning electron microscopy to investigate microstructures of composites with varying PWA content. Impedance measurements and diffusion cell tests were also made to determine the proton conductivity and the ethanol permeability. The performances of proof-of-concept fuel cells that incorporate the PWA–Nafion composites were compared. The results presented here demonstrate that the addition of PWA into Nafion membrane significantly reduces the ethanol-crossover in direct ethanol fuel cell application, and this improvement in fuel crossover contributes to the enhancement of device performance.

## Experimental details

### Synthesis of PWA–Nafion composites

A series of PWA-added Nafion composite membranes was prepared as a function of PWA concentration. Nafion ionomer dispersion (10 wt% solution in H<sub>2</sub>O, Iko Chemical) and phosphotungstic acid hydrate (H<sub>3</sub>[P(W<sub>3</sub>O<sub>10</sub>)<sub>4</sub>] · *x*H<sub>2</sub>O, Sigma Aldrich) were used without any further purification. Various mixtures of PWA/Nafion (0/100, 5/95, 10/90, 15/85, 20/80) in weight fraction (wt%) were prepared. The synthesis of PWA–Nafion composites is schematically illustrated in Fig. 1: (a) Nafion ionomer dispersion is dried in a vacuum oven at 80 °C for 5 h in order to evaporate solvents. (b) The resulting solid-phase Nafion and PWA particles are then dissolved in dimethylformamide (DMF, (CH<sub>3</sub>)<sub>2</sub>NC(O)H, JUNSEI) for 24 h under stirring. (c) Then, the PWA–Nafion solution is poured into the flat and smooth casting mold. (d) By casting solution in a vacuum oven at 80 °C for 12 h and curing at 120 °C for 6 h, (e) the PWA-added Nafion membranes are obtained. Nafion-117 (Iko Chemical), the commercial Nafion membrane widely used for DAFC, was also processed as a reference. In order to convert membranes into acid form (i.e., –SO<sub>3</sub><sup>–</sup> H<sup>+</sup>) before characterizations, the membranes were

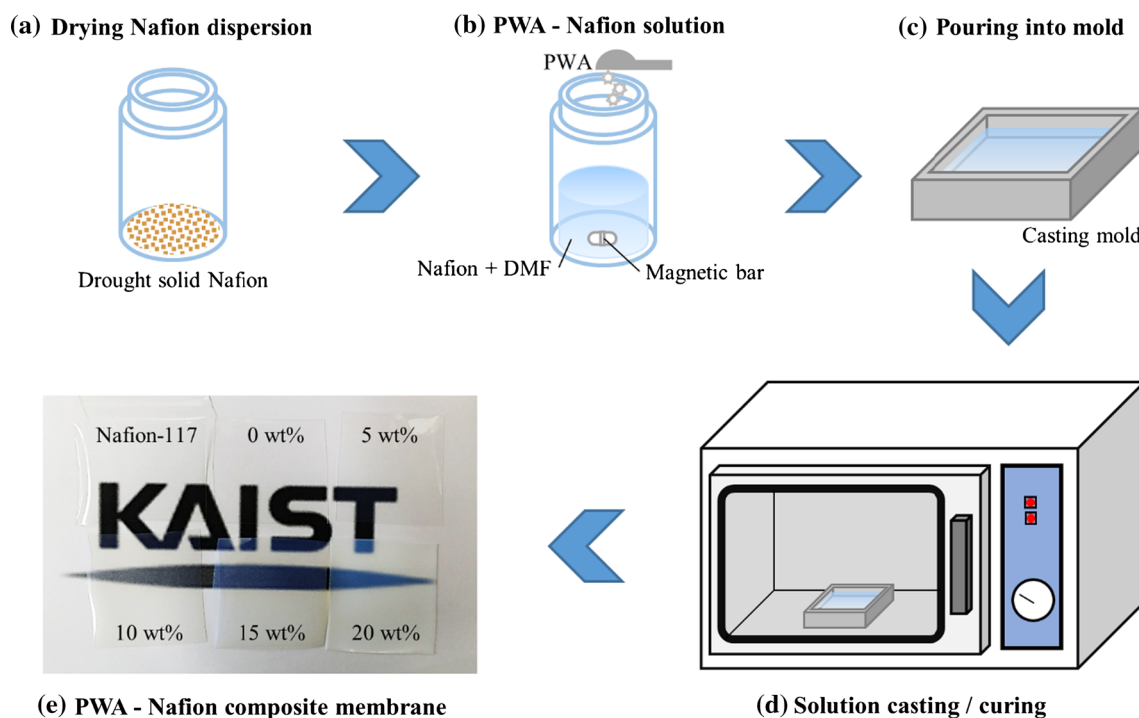


**Figure 1** Schematic of method to fabricate PWA–Nafion composite membranes.

pretreated by boiling them in 1 M aqueous sulfuric acid solution at 80 °C, deionized water, in that order.

### Characterizations of PWA–Nafion composites

The morphology and microstructure of the PWA/Nafion membranes were characterized using Hitachi S-4800 scanning electron microscope (SEM) to investigate the effect of the addition of PWA particles on the uniformity of the resulting composites and the evolution of microstructure. X-ray diffraction (XRD) measurements were carried out in a Rigaku Ultima IV in order to evaluate amorphous/crystalline structure of the materials using Cu  $K\alpha$  radiation ( $\lambda$ -0.154 nm) at 30 kV and 60 mA. The XRD spectra were obtained at diffraction angles ( $2\theta$ ) ranging from 2° to 60° with a scan rate of 3°/min. A diffusion cell method was used to evaluate the permeability of the PWA–Nafion membranes. The diffusion cell was separated by the membrane and each chamber was filled with ethanol aqueous solution (2.0 mol/L, neutral) and deionized water, respectively. The homogeneity of solutions in the cell chambers was ensured by stirring chambers using magnetic bars during permeability measurements. The ethanol concentration of sample solutions taken from the cell

chamber was monitored using an Atago PAL-34S digital ethanol meter.

Water uptake tests were made on the PWA–Nafion composites in order to investigate the effect of PWA additives on the hydration behavior of the membranes. Before the test, all samples were dried in a vacuum oven at 70 °C for 12 h to exclude the effect of pre-adsorbed water on the evaluation. The fully dried samples were then weighed (dry weight,  $W_{\text{dry}}$ ) and soaked in deionized water for a day so that the membranes can inhale water. After taking out samples from water, a tissue paper was used to remove droplets on the surface and the membranes were weighed (wet weight,  $W_{\text{wet}}$ ) again, and then compared with  $W_{\text{dry}}$ . The proton conductivity of the membranes was examined by a four-contact ac impedance measurement technique using Bio-Logic VSP-3000 impedance analyzer at an amplitude of 10 mV with the frequencies ranging from 7 MHz to 0.1 Hz. The conductivity measurements were performed at 65 °C under the fully hydrated state.

### Performance of the DEFC utilizing PWA–Nafion composite membranes

The gas diffusion electrodes (GDE, NARA Celtech) coated with 40% Pt–Ru/C and 40% Pt/C catalyst

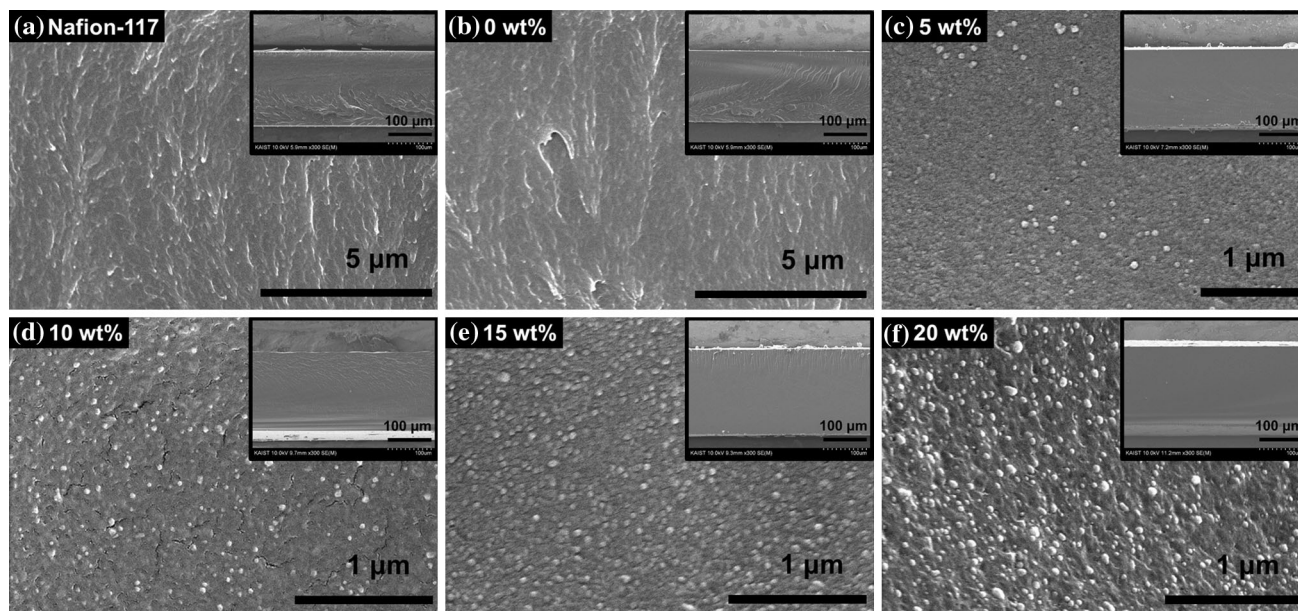


**Figure 2** Cross-sectional SEM images of the **a** commercial Nafion-117, the PWA–Nafion composite membrane, where the weight percent of PWA particles of **b** 0 wt%, **c** 5 wt%, **d** 10 wt%, **e** 15 wt%, and **f** 20 wt%. *Insets* are low-magnification images of the membranes.

were used as the anode and cathode, respectively. Both electrodes were loaded with  $0.5 \text{ mg/cm}^2$  catalysts. The PWA-added membranes prepared in this study were used as the electrolyte membrane, and the commercial Nafion-117 was also used as a reference. A set of membrane electrode assemblies (MEAs) with the effective cell area of  $9 \text{ cm}^2$  was fabricated by hot pressing at  $140 \text{ }^\circ\text{C}$  for 150 s. The performance of these prototype devices was characterized in a fuel cell station (Smart2, Won A Tech) at 70, 80, and  $90 \text{ }^\circ\text{C}$  with 2.0 M ethanol aqueous solution (neutral) at a flow rate of 2 mL/min and high-purity oxygen (99.999%) at a flow rate of 400 ccm. The cell performance was evaluated without back pressure.

## Results and discussion

A series of PWA-added Nafion membranes was fabricated using solution casting as a function of PWA concentration (0, 5, 10, 15, and 20 wt% PWA). The properties of PWA–Nafion composite membranes and the performance of fuel cell devices were systematically evaluated and compared with those of commercial Nafion-117. As a figure of merit, properties and performance of various membranes with a similar thickness of approximately 180–190  $\mu\text{m}$  will be compared.

### Microstructure of PWA–Nafion composites

Figure 2 shows the cross-sectional scanning electron microscope (SEM) images of Nafion-117 as a reference and prepared PWA–Nafion membranes with PWA concentrations ranging from 0 to 20 wt%. Each inset shows a low-magnification SEM image from which the membrane thickness ( $\sim 190 \mu\text{m}$ ) is estimated. No significant microstructure difference is observed between commercial Nafion-117 (Fig. 2a) and 0 wt%-PWA–Nafion (Fig. 2b) fabricated in this study. In Fig. 2c, the appearance of new features is clearly detected, which is attributed to the incorporation of 5 wt% of PWA in Nafion. X-ray diffraction analysis for the identification of PWA structure will be further discussed in the following section. The amount of the white phase increases with increasing PWA concentration as presented in Fig. 2c–f and the images present that the PWA is uniformly distributed in the entire sample, whose excellent uniformity is favorable for fuel cell device application.

### X-ray diffraction analysis

Figure 3 shows the  $\theta$ – $2\theta$  coupled scan X-ray diffraction patterns of the PWA–Nafion composites fabricated on slide glass substrates. Typical XRD spectra of commercial Nafion-117 (bottom curve) and

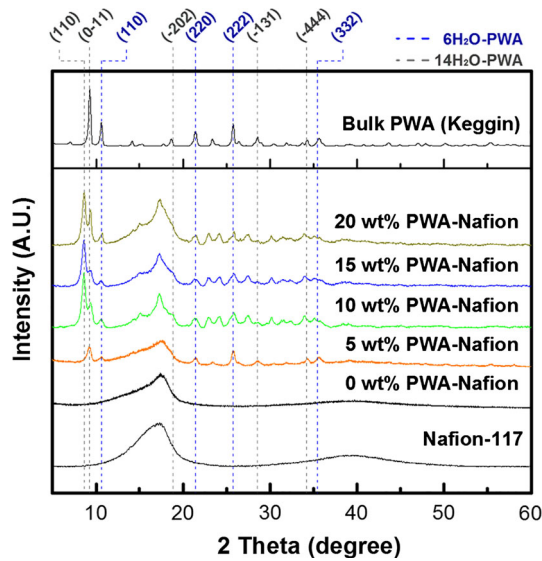


**Figure 3** X-ray diffraction patterns of the PWA–Nafion composites and references commercial of Nafion-117 and bulk PWA.

bulk PWA powder (top curve) are also presented as references. Nafion-117 presents the prominent broad spectra at diffraction angle,  $2\theta \sim 12^\circ\text{--}20^\circ$ , which is attributed to mixed crystalline and amorphous phases and another broad peak (weak) is also seen at  $2\theta = 35^\circ\text{--}43^\circ$ . The characteristic diffraction peaks, known as cubic-phase Keggin structure, of bulk PWA are shown in the top of Fig. 3 [31]. Note that the bulk PWA XRD patterns consist of two hydrate states of  $14\text{H}_2\text{O-PWA}$  and  $6\text{H}_2\text{O-PWA}$ . Mioc et al. [31]. reported that the hydrate state (i.e., the number of water molecules) in PWA decreases with increasing temperature during thermal process (e.g., pre- or post-annealing) and the different hydrate states lead to shifts and changes in diffraction patterns. In this study,  $6\text{H}_2\text{O-PWA}$  results in diffraction peaks from (110), (220), (222), and (332) at  $2\theta = 10.6^\circ, 21.4^\circ, 25.8^\circ,$  and  $35.6^\circ$  [31], while  $14\text{H}_2\text{O-PWA}$  yields peaks of (0–11), (–202), (–131), and (–4–44) at  $2\theta = 9.3^\circ, 18.7^\circ, 28.6^\circ,$  and  $34.3^\circ$ , respectively, with other minor diffractions at  $\sim 20^\circ\text{--}35^\circ$ , which are difficult to index due to the diffraction overlaps of 14- and  $6\text{H}_2\text{O-PWA}$ . The XRD spectra obtained from PWA–Nafion composites clearly present that the PWA additives have been well incorporated in the composite membranes maintaining Keggin structure. All PWA-added Nafion membranes present  $6\text{H}_2\text{O-PWA}$  (110), (220), (222), and (332) as well as  $14\text{H}_2\text{O-PWA}$  (0–11), (–131), and (–4–44). It should be noted, however, that a strong diffraction intensity of  $14\text{H}_2\text{O-PWA}$

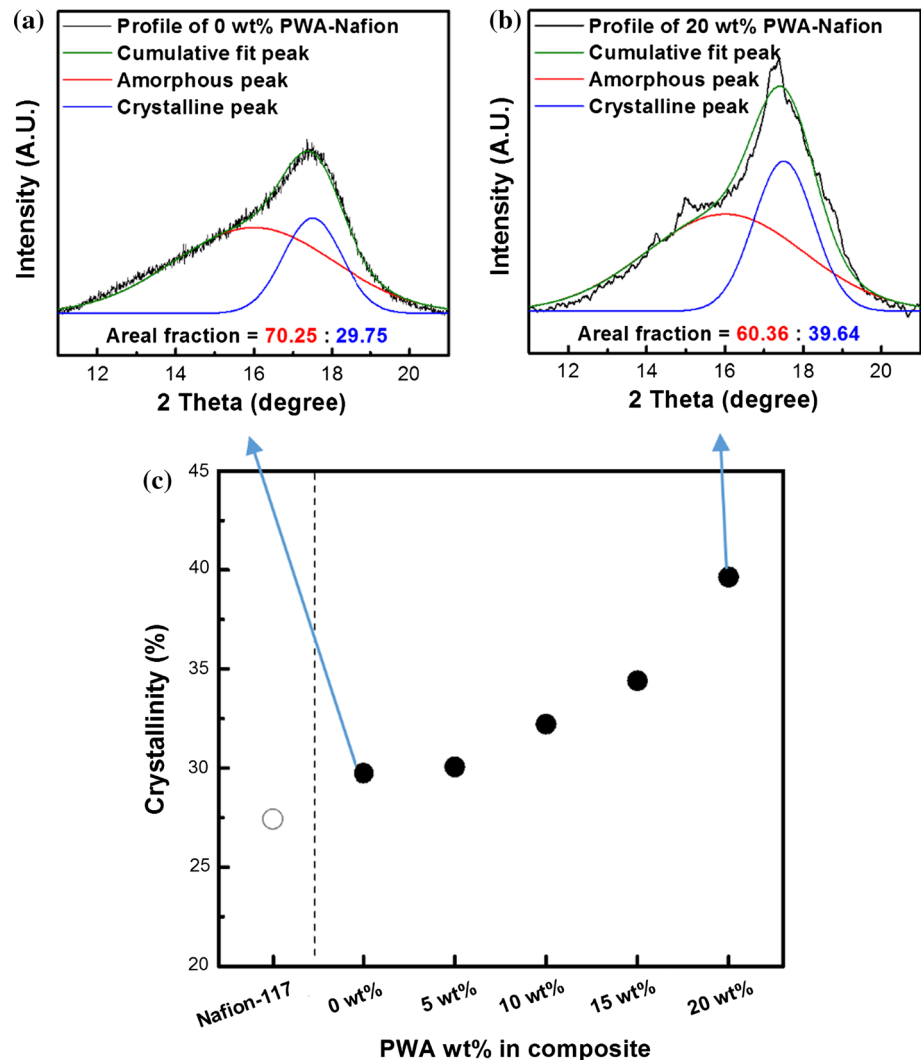
(110) is detected from the PWA–Nafion composites with 10, 15, and 20 wt% PWA, which is not observed in 5 wt% PWA–Nafion. This difference in diffraction spectra between 5 wt% and higher (10–20 wt%) PWA–Nafion is likely attributed to the fact that the lattice strain and distortion increase with increasing PWA content, which may limit a reduction in hydrate state of higher PWA concentration samples. The greater hydrate states shown in higher PWA concentration membranes are possibly associated with the similar amount of water uptake shown in Fig. S1 in spite of the enhanced crystallinity with increasing PWA content (i.e., decrease in the volume fraction of hydrophilic region).

In Fig. 3, the diffraction intensity of both Keggin structure and Nafion is evidently increased with increasing PWA concentration in the PWA–Nafion composite membranes. In particular, the enhancement of Nafion crystallinity, which is of relevance to the ethanol-crossover, is quantified by evaluating areal fractions between crystalline and amorphous phases from the peak diffracted at  $2\theta = 12^\circ\text{--}20^\circ$  [32]: each peak was decomposed into two diffractions of amorphous phase ( $2\theta \sim 16^\circ$ ) due to hydrophilic region and crystalline phase ( $2\theta \sim 17.5^\circ$ ) attributed to hydrophobic perfluorocarbon backbone chains of Nafion structure, respectively [32]. The percent crystallinity was investigated using the Eq. (1):

$$\text{Crystallinity (\%)} = \frac{A_c}{A_c + A_a} \times 100, \quad (1)$$

where  $A_c$  and  $A_a$  are the areas of crystalline and amorphous peaks, respectively. The decomposed diffraction spectra of the 0 and 20 wt% PWA–Nafion composites are shown in Fig. 4a, b where the areal fraction of crystalline state in 20 wt% PWA composite is found to be approximately 40%, while that of 0 wt% (no PWA added) sample is  $\sim 30\%$ . The calculated crystallinity of all samples prepared in this study as well as commercial Nafion is shown in Fig. 4c. The crystallinity of the 20 wt% PWA–Nafion composite showed an approximately 33% increase compared to those of 0 wt% PWA–Nafion and commercial Nafion-117 membranes. This is likely due to the additional nucleation sites by the incorporation of PWA into Nafion that facilitate crystallization during solidification of PWA–Nafion solution. Since crystalline Nafion is more hydrophobic than that in amorphous state, which may limit the diffusion of water and ethanol through the membrane, an

**Figure 4** Determination of the crystallinity (%) of Nafion by comparing areal fraction of crystalline and amorphous phases from the peak at  $2\theta \sim 12^\circ\text{--}20^\circ$ : decomposed peaks of **a** 0 wt% and **b** 20 wt% PWA–Nafion membranes are presented and **c** crystallinity of all samples is shown as a function of PWA concentration with the reference of commercial Nafion-117.



increase in the crystallinity with increasing PWA concentration may lead to a reduction in ethanol-crossover in DEFC application [12].

### Determination of diffusion coefficient

Since the diffusion coefficient is the property that describes the permeability of an element within another (i.e., membrane in this study), the determination of diffusion coefficient of the PWA–Nafion membranes allows for the direct investigation of the ability to mitigate ethanol-crossover. The ethanol diffusion coefficient ( $P$ ) was evaluated using a diffusion cell and Eq. (2):

$$C_B(t) = \frac{APC_A t}{V_B L}, \quad (2)$$

where  $C_A$  and  $C_B$  are the feed and permeated ethanol concentrations, respectively,  $V_B$  the volume of liquid permeated,  $L$  the thickness of membrane,  $A$  the effective area of membrane, and  $t$  is the elapsed diffusion time. Figure 5 indicates that the diffusion coefficient significantly decreases with increasing PWA concentration, from 1.53 (0 wt% PWA) to 1.06 (20 wt%-PWA). Note that our PWA–Nafion composites (10, 15, and 20 wt% PWA) present greater ability to prevent ethanol-crossover than that of the commercial Nafion-117, while 5 wt% PWA–Nafion show comparable performance. Previously, Xiang et al. [23] reported the effect of the PWA incorporation on direct methanol fuel cells. They suggested that PWA in Nafion narrows the methanol diffusion channel whose reduced channel volume improves

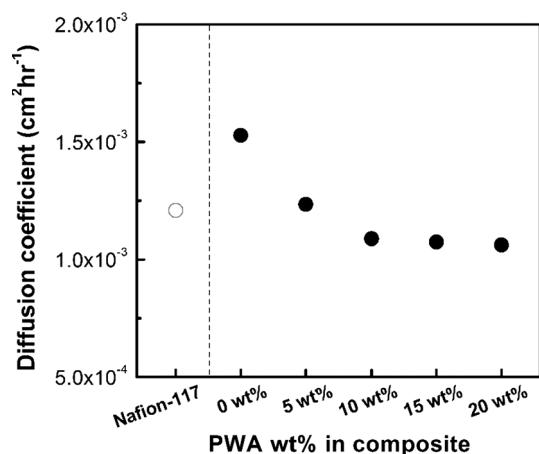


**Figure 5** Ethanol diffusion coefficients of PWA–Nafion composite membranes measured in a diffusion cell at room temperature. The results present that the diffusion coefficient decreases with increasing PWA concentration, and 10, 15, and 20 wt% PWA–Nafion composites show lower values of  $\sim 1.06 \text{ cm}^2 \text{ h}^{-1}$  than  $\sim 1.25 \text{ cm}^2 \text{ h}^{-1}$  of Nafion-117, which indicates that the ability to limit ethanol-crossover improves with increasing PWA content, and PWA–Nafion membranes demonstrate greater ethanol-blocking property than commercial Nafion.

methanol-block properties. Similarly, the improvement of ethanol-crossover shown in the present study is likely attributed to a reduction in the volume of the water channel by the addition of the PWA particles which efficiently suppress the diffusion of ethanol molecules. This enhanced ethanol-crossover due to reduced channel volume can be understood in Eq. (2), where smaller  $V_B$  yields lower diffusion coefficient,  $P$ , which is also supported by the XRD results (Fig. 4c) that exhibit the increase in crystalline phase with increasing PWA concentration.

### Impedance spectroscopy measurement and selectivity factor

In order to determine proton conductivity of the membrane, impedance spectroscopy measurements were performed in a membrane conductivity measuring cell (MCC, Won A Tech) with four platinum wires for contacts. Figure 6 presents the resulting proton conductivity of PWA–Nafion membranes and the inset shows a photo of the cell with a mounted membrane that we used in this study. The proton conductivity ( $\sigma$ ) of the membranes was measured using Ohm's law (Eq. 3):

$$\sigma = \frac{L}{RA}, \quad (3)$$

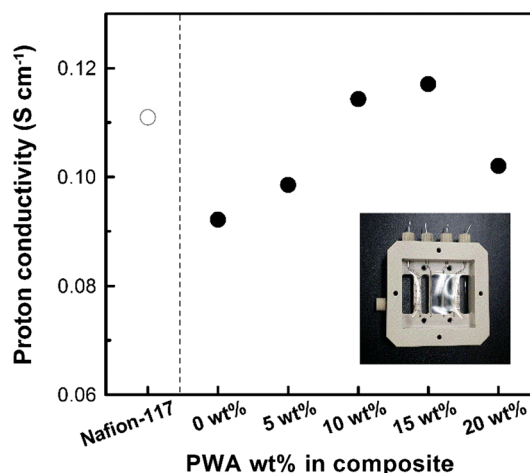


**Figure 6** Plot of proton conductivity of PWA–Nafion composites versus PWA content measured at 65 °C: the conductivity increases with increasing PWA content until 15 wt% from  $\sim 0.09$  (0 wt%) to  $0.12 \text{ S cm}^{-1}$ , which is higher than  $\sim 0.11 \text{ S cm}^{-1}$  of commercial Nafion-117, and then decreases toward  $0.10 \text{ S cm}^{-1}$  (20 wt%). *Inset* is a photograph of membrane conductivity measuring cell which shows that a PWA–Nafion sample is mounted on the cell.

where  $L$  is the length between the two probes,  $R$  is the measured sample resistance, and  $A$  is the cross-sectional area of the sample. At PWA concentrations ranging from 0 to 15 wt%, the proton conductivity of PWA–Nafion composites increases with increasing PWA content from approximately  $0.09 \text{ Scm}^{-1}$  (0 wt%) to  $0.12 \text{ Scm}^{-1}$  (15 wt%), which is the maximum value achieved in this study and is slightly higher than  $\sim 0.11 \text{ Scm}^{-1}$  of commercial Nafion-117. At a higher PWA concentration of 20 wt%, a decrease in conductivity, which is the opposite trend, was observed.

It is widely believed that the enhanced ability to contain water (i.e., water uptake) improves the proton conductivity. Amirinejad et al. [33]. reported that the incorporation of cesium hydrogen salt of heteropolyacid to Nafion increases the percent water uptake by providing additional hydrophilic water channel that facilitates proton conduction and consequently leads to an increase in proton conductivity. This insertion is known as the vehicular model that supports the improved proton conductivity due to an increase in volume fraction in water channel. In the present study, however, the measured water uptake values of PWA–Nafion composites (see Fig. S1 in supporting information) are nearly constant and, therefore, the enhanced proton conductivity with



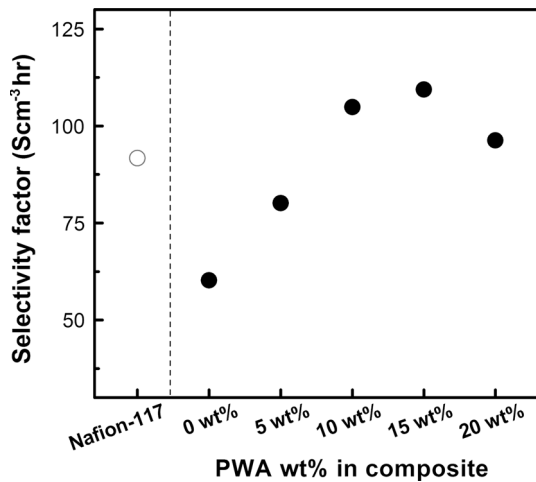


**Figure 7** Selectivity factor of PWA–Nafion composite membranes calculated from the proton conductivity measured at 65 °C and the ethanol diffusion coefficient of each membrane. The composite with 15 wt% PWA particles exhibits the highest value of 109.39 S cm<sup>-3</sup> h.

increasing PWA content is not attributed to the increased water channel volume [34, 35]. Instead, an increase in proton conductivity until the PWA content of 15 wt% is possibly due to the creation of efficient proton hopping pathway provided by inherent high ionic conducting nature of hydrophilic PWA particles in membranes [36]. In our PWA–Nafion composite membranes, uniformly distributed PWA particles inside or near the ion channels (i.e., hydrophilic region that protons pass through) may form bridges between (SO<sub>3</sub><sup>-</sup>) ions and consequently enhance proton transports by reducing hopping distance between ions. This process is termed Grotthuss diffusion [34], in which proton transport depends on hopping between molecules or SO<sub>3</sub><sup>-</sup> ions at inner wall of hydrophilic region, rather than water volume fraction in membranes. This PWA-induced enhancement in hopping conduction in Nafion is supported by the recent study by Lu. et al. who reported that a significant increase in proton conductivity of the PWA–Nafion multilayer membrane is associated with the enhanced hopping conduction by generating ion bridges using ion-conductive PWA particles [26]. Note that a decrease in proton conductivity was observed in the 20 wt% PWA–Nafion. This reverse trend is likely because excessive PWA particles tend to aggregate inhomogeneously [37] and lead to the formation of relatively large PWA particles, as shown in SEM image Fig. 2f. The excess and inhomogeneous

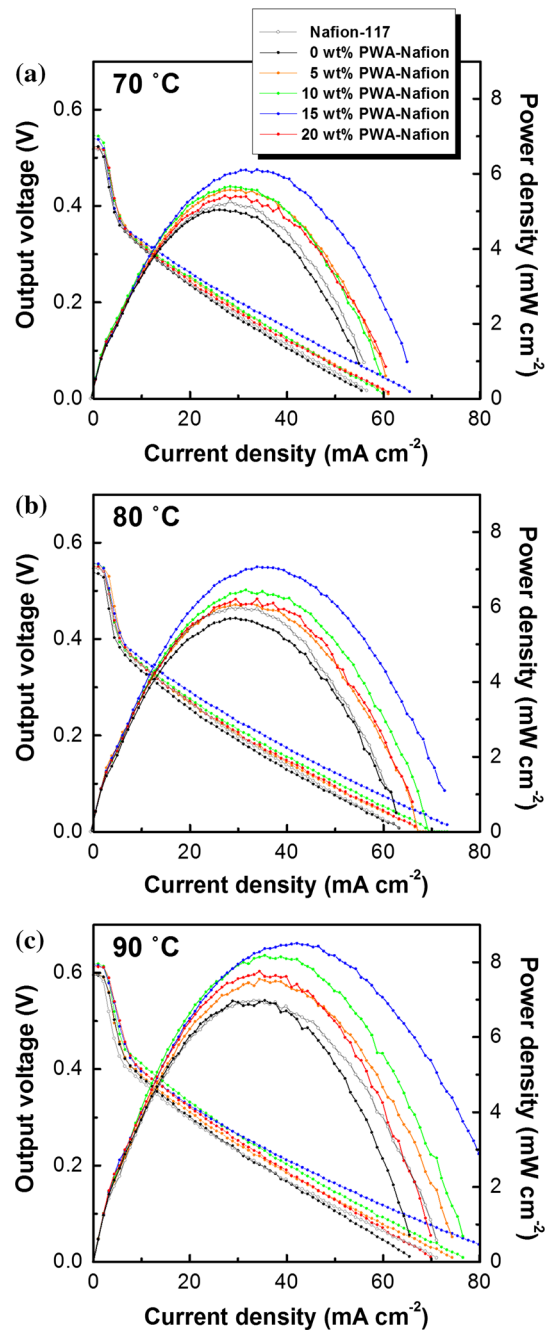


**Figure 8** *I*–*V* characteristics of DEFCs utilizing PWA–Nafion composites as a membrane (with Pt–Ru/C anode and Pt/C cathode): plots of output voltage and power density are presented as a function of current density at temperatures of **a** 70 °C, **b** 80 °C, and **c** 90 °C. The cells were fed with 2.0 M ethanol aqueous solution as a fuel at a flow rate of 2 mL/min and high-purity oxygen at a flow rate of 400 ccm.

PWA may limit the continuum of water cluster and proton transport [12, 29].

Selectivity factor ( $\Phi$ ) is often used as a crude indicator of the overall membrane performance for fuel

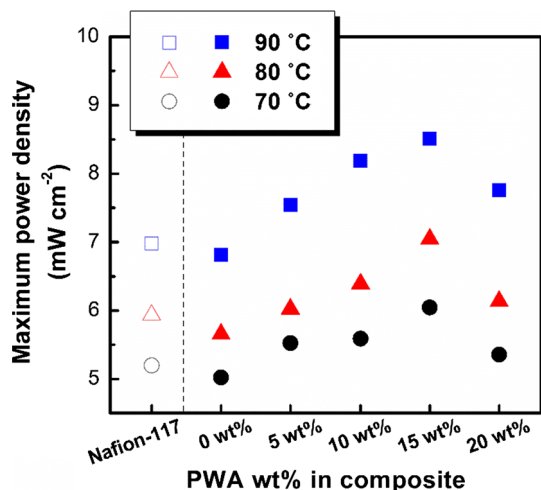


**Figure 9** Maximum power density of PWA–Nafion DEFCs extracted from the  $I$ – $V$  characteristics which summarizes the DEFC performance: although undoped (0 wt% PWA) Nafion shows slightly lower maximum power density compared to that of commercial Nafion-117 device, other devices using 5, 10, 15, and 20 wt% PWA–Nafion exhibit higher performance than Nafion-117. Among PWA–Nafion DEFCs, the maximum power density increases with increasing PWA concentration until 15 wt% and then decreases, which is a similar trend observed in the proton conductivity.

cell application. The factor is simply determined from Eq. (4):

$$\Phi = \sigma/P, \quad (4)$$

where  $\sigma$  is the proton conductivity and  $P$  is the ethanol diffusion coefficient. Since a higher selectivity factor indicates higher proton conductivity and alleviated fuel crossover of the membrane, higher  $\Phi$  represents higher cell performance of DEFCs than those with lower  $\Phi$ . As shown in Fig. 7, the membrane with the PWA content of 15 wt% exhibited the highest  $\Phi$  value.

### Single-cell performance test

The PWA–Nafion composites prepared in this study and a commercial Nafion-117 (as a reference) were incorporated in DEFCs as a membrane, and the device performance was evaluated at temperatures of 70, 80, and 90 °C. The plots of cell voltage and power density versus current density of DEFCs are presented as a function of PWA concentration in Fig. 8a–c measured at 70, 80, and 90 °C, respectively. It should be noted that DEFCs utilizing PWA-added Nafion membranes (5, 10, 15, and 20 wt%) clearly

exhibit higher output voltages and power density than those of the commercial Nafion-117 DEFC and pure Nafion DEFC casted in this study. The fuel cell power density increases with increasing PWA concentration until 15 wt% of PWA in the composites and the device with 20 wt% PWA–Nafion slightly decreases compared to that of 15 wt% PWA–Nafion DEFC due to the relatively low proton conductivity of 20 wt% PWA–Nafion membrane. The open circuit voltage (OCV) increases with increasing temperature from  $\sim 0.5$  V measured at 70 °C to  $>0.6$  V at 90 °C. This enhancement in OCV is likely associated with the enhanced electrochemical reactions in the electrodes due to an increase in thermal activation at higher temperatures [7, 38]. The alteration of OCVs as a function of PWA concentration shows no significant dependence on the ethanol permeability shown in Fig. 5. This can be understood by that the OCV of the devices is determined by the overall effect of various parameters (e.g., operation condition, interlayers of MEA, catalyst layer, hot-pressed condition, proton conductivity, ethanol permeability, series resistance of the devices) rather than solely by the ethanol permeability.

The maximum power density (Max P) of this set of DEFCs is shown in Fig. 9. The Max P of the DEFCs and the percent increase in Max P compared to the commercial Nafion-117 device are summarized in Table 1. The Max P of the commercial Nafion-117 DEFC was 5.19, 5.93, and 6.98  $\text{mW cm}^{-2}$  at 70, 80, and 90 °C, respectively. The cell with the 15 wt% PWA–Nafion composite exhibited the best performance with the highest Max P among all DEFCs in this study, which was 6.04, 7.04, and 8.51  $\text{mW cm}^{-2}$  at 70, 80, and 90 °C which were 16.49, 18.73, and 21.97% higher than those of commercial Nafion-117 DEFCs, respectively. This performance improvement is attributed to the reduced ethanol-crossover and enhanced crystalline structure as well as higher proton conductivity of the PWA–Nafion composites. In Fig. 10, the maximum power density of 15 wt% PWA–Nafion DEFC was plotted in log scale on a conventional Arrhenius plot as a function of inverse absolute temperatures, where the power density was clearly shown to be thermally activated and the activation energy for the maximum power density was determined to be 0.18 eV. This low activation energy is of great importance to high-performance fuel cell application that is operated at reasonably low temperatures.

**Table 1** The maximum power density of PWA–Nafion DEFCs as a function of PWA concentration and an increase of each DEFC compared to commercial Nafion-117 DEFC: PWA-added

Membranes	70 °C		80 °C		90 °C	
	Max P (mW cm <sup>-2</sup> )	Increase (%)	Max P (mW cm <sup>-2</sup> )	Increase (%)	Max P (mW cm <sup>-2</sup> )	Increase (%)
Nafion-117	5.19	–	5.93	–	6.98	–
0 wt%	5.02	–3.21	5.66	–4.68	6.81	–2.38
5 wt%	5.52	6.42	6.02	1.5	7.54	8.12
10 wt%	5.59	7.71	6.39	7.68	8.19	17.35
15 wt%	6.04	16.49	7.04	18.73	8.51	21.97
20 wt%	5.36	3.21	6.13	3.37	7.76	11.15

(5, 10, 15, 20 wt%) Nafion DEFCs present higher Max P than those of commercial Nafion devices

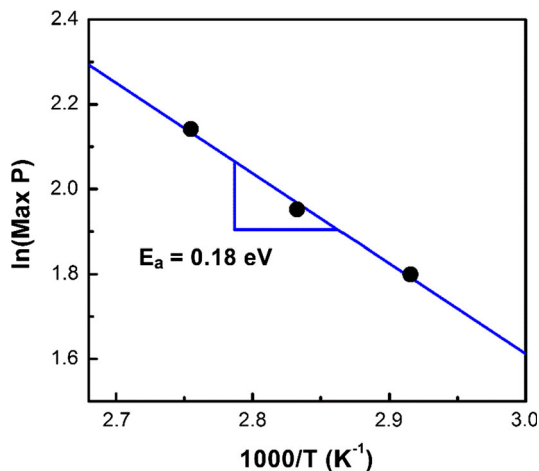


**Figure 10** Arrhenius plot of maximum power density in log scale vs reciprocal temperature where the activation energy for a change in power density is found to be 0.18 eV.

Achieving stable performance of the materials and the devices over time in ambient conditions is the next challenging issue for the implementation of PWA–Nafion composites for fuel cell application as unfavorable fuel cell performance degradation has been reported. This performance instability is mainly attributed to a leaching of PWA particles resulting from the soluble nature of PWA. The performance degradation due to the leaching issue is likely reduced by anchoring PWA on supporting agents which have strong interactions with PWA, such as silica [36, 39], zirconia [18, 29], and cesium ion (Cs<sup>+</sup>) [23, 33]. As suggested by Yang et al. [24], the addition of poly-diallyldimethylammonium chloride that enables PWA to be trapped on Nafion surface can also be favorable to improve the performance degradation observed in the fuel cell performance [24].

## Conclusion

In this work, we have reported the effect of PWA content in PWA–Nafion composite membrane on the ethanol-crossover and proton conduction in DEFC application. The ability to block ethanol-crossover is significantly improved with increasing PWA in PWA–Nafion membrane: PWA (20 wt%)-Nafion shows 12.2% lower ethanol permeability than that of pure Nafion membrane. This improvement is likely related to the results of XRD test, which shows increased crystallinity of the membranes with increasing PWA content. This relationship between crystallinity and PWA content is likely attributed to the additional nucleation sites provided by PWA particles during solidification of Nafion solution. An increase in volume of hydrophobic crystalline phase in the PWA–Nafion composites narrows the water channel, thus improving ethanol-crossover. The single-cell DEFC measurements reveal that the maximum power density of the 15 wt% PWA–Nafion composite membranes is considerably improved by 22% higher than that of Nafion-117 DEFC, which is due to the improvements in ethanol-crossover and proton conductivity of the composite membrane. The potentials to further enhance ethanol-blocking ability and proton conductivity of PWA–Nafion composites can motivate further research on the development of composite membranes and the performance improvement of non-toxic and cost-effective direct ethanol fuel cell devices.

## Acknowledgements

The authors gratefully thank the Mid-career Researcher Program (No. 2010-0015063) and Conversion Research

Center Program (No. 2011K000674) through the National Research Foundation of Korea (NRF) funded by the Ministry of Education, Science and Technology (MEST) and Basic Science Research Program (No. 2015R1D1A1A01056983) through the NRF, Korea, funded by the Ministry of Education for the financial support. S.L. acknowledges Baylor University faculty startup funds that supported this research. The work at Argonne (S.H., data analysis and contribution to manuscript writing) was supported by U.S. Department of Energy, Office of Basic Energy Sciences, Materials Sciences and Engineering Division. The authors also acknowledge technical support from the K-LAB.

### Compliance with ethical standards

**Conflict of interest** The authors declare no competing financial interest.

**Electronic supplementary material:** The online version of this article (doi:[10.1007/s10853-016-0534-z](https://doi.org/10.1007/s10853-016-0534-z)) contains supplementary material, which is available to authorized users.

### References

- [1] Li X, Faghri A (2013) *J Power Sour* 226:223–240. doi:[10.1016/j.jpowsour.2012.10.061](https://doi.org/10.1016/j.jpowsour.2012.10.061)
- [2] Sharaf OZ, Orhan MF (2014) *Renew Sust Energy Rev* 32:810–853. doi:[10.1016/j.rser.2014.01.012](https://doi.org/10.1016/j.rser.2014.01.012)
- [3] Han I-S, Kho B-K, Cho S (2016) *J Power Sour* 304:244–254. doi:[10.1016/j.jpowsour.2015.11.049](https://doi.org/10.1016/j.jpowsour.2015.11.049)
- [4] Antonucci PL, Aricò AS, Creti P, Ramunni E, Antonucci V (1999) *Solid State Ion* 125:431–437. doi:[10.1016/S0167-2738\(99\)00206-4](https://doi.org/10.1016/S0167-2738(99)00206-4)
- [5] Kua J, Goddard WA (1999) *J Am Chem Soc* 121:10928–10941. doi:[10.1021/ja9844074](https://doi.org/10.1021/ja9844074)
- [6] Wen Z, Liu J, Li J (2008) *Adv Mater* 20:743–747. doi:[10.1002/adma.200701578](https://doi.org/10.1002/adma.200701578)
- [7] Zhou W, Zhou Z, Song S et al (2003) *Appl Catal B* 46:273–285. doi:[10.1016/S0926-3373\(03\)00218-2](https://doi.org/10.1016/S0926-3373(03)00218-2)
- [8] Rousseau S, Coutanceau C, Lamy C, Léger JM (2006) *J Power Sour* 158:18–24. doi:[10.1016/j.jpowsour.2005.08.027](https://doi.org/10.1016/j.jpowsour.2005.08.027)
- [9] Badwal SPS, Giddey S, Kulkarni A, Goel J, Basu S (2015) *Appl Energy* 145:80–103. doi:[10.1016/j.apenergy.2015.02.002](https://doi.org/10.1016/j.apenergy.2015.02.002)
- [10] Zakaria Z, Kamarudin SK, Timmiati SN (2016) *Appl Energy* 163:334–342. doi:[10.1016/j.apenergy.2015.10.124](https://doi.org/10.1016/j.apenergy.2015.10.124)
- [11] Pethaiah SS, Arunkumar J, Ramos M, Al-Jumaily A, Manivannan N (2016) *Bull Mater Sci*. doi:[10.1007/s12034-015-1130-6](https://doi.org/10.1007/s12034-015-1130-6)
- [12] Barbara L, Charya SA, Verna A (2009) *Macromol Symp* 277:177–189. doi:[10.1002/masy.200950322](https://doi.org/10.1002/masy.200950322)
- [13] Battiroli LC, Schneider JF, Torriani ÍCL, Tremiliosi-Filho G, Rodrigues-Filho UP (2013) *Int J Hydrog Energy* 38:12060–12068. doi:[10.1016/j.ijhydene.2013.06.126](https://doi.org/10.1016/j.ijhydene.2013.06.126)
- [14] Maab H, Nunes SP (2010) *J Power Sour* 195:4036–4042. doi:[10.1016/j.jpowsour.2010.01.005](https://doi.org/10.1016/j.jpowsour.2010.01.005)
- [15] Kozhevnikov IV (1998) *Chem Rev* 98:171–198
- [16] Misono M (1987) *Catal Rev* 29:269–321. doi:[10.1080/01614948708078072](https://doi.org/10.1080/01614948708078072)
- [17] Amirinejad M, Madaeni SS, Navarra MA, Rafiee E, Scrosati B (2011) *J Power Sour* 196:988–998. doi:[10.1016/j.jpowsour.2010.08.062](https://doi.org/10.1016/j.jpowsour.2010.08.062)
- [18] Saccà A, Carbone A, Pedicini R et al (2008) *Fuel Cells* 8:225–235. doi:[10.1002/fuce.200800009](https://doi.org/10.1002/fuce.200800009)
- [19] Bakangura E, Wu L, Ge L, Yang Z, Xu T (2016) *Prog Polym Sci* 57:103–152. doi:[10.1016/j.progpolymsci.2015.11.004](https://doi.org/10.1016/j.progpolymsci.2015.11.004)
- [20] Horan JL, Genupur A, Ren H et al (2009) *ChemSusChem* 2:226–229. doi:[10.1002/cssc.200800237](https://doi.org/10.1002/cssc.200800237)
- [21] Horan JL, Lingutla A, Ren H et al (2014) *J Phys Chem C* 118:135–144. doi:[10.1021/jp4089657](https://doi.org/10.1021/jp4089657)
- [22] Motz AR, Horan JL, Kuo M-C, Herring AM (2015) *ECS Trans* 69:587–590. doi:[10.1149/06917.0587ecst](https://doi.org/10.1149/06917.0587ecst)
- [23] Xiang Y, Yang M, Zhang J, Lan F, Lu S (2011) *J Membr Sci* 368:241–245. doi:[10.1016/j.memsci.2010.11.049](https://doi.org/10.1016/j.memsci.2010.11.049)
- [24] Yang M, Lu S, Lu J, Jiang SP, Xiang Y (2010) *Chem Commun* 46:1434–1436. doi:[10.1039/b912779h](https://doi.org/10.1039/b912779h)
- [25] Malhotra S, Datta R (1997) *J Electrochem Soc* 144:L23–L26. doi:[10.1149/1.1837420](https://doi.org/10.1149/1.1837420)
- [26] Lu JL, Fang QH, Li SL, Jiang SP (2013) *J Membr Sci* 427:101–107. doi:[10.1016/j.memsci.2012.09.041](https://doi.org/10.1016/j.memsci.2012.09.041)
- [27] Abouzari-lotf E, Jacob MV, Ghassemi H et al (2016) *J Power Sour* 326:482–489. doi:[10.1016/j.jpowsour.2016.07.027](https://doi.org/10.1016/j.jpowsour.2016.07.027)
- [28] Abouzari-lotf E, Nasef MM, Ghassemi H, Zakeri M, Ahmad A, Abdollahi Y (2015) *ACS Appl Mater Interfaces* 7:17008–17015. doi:[10.1021/acsami.5b02268](https://doi.org/10.1021/acsami.5b02268)
- [29] Carbone A, Casciola M, Cavalaglio S et al (2004) *J N Mater Electrochem Syst* 7:1–5
- [30] Xu W, Lu T, Liu C, Xing W (2005) *Electrochim Acta* 50:3280–3285. doi:[10.1016/j.electacta.2004.12.014](https://doi.org/10.1016/j.electacta.2004.12.014)
- [31] Mioč UB, Dimitrijević RŽ, Davidović M, Nedić ZP, Mitrović MM, Colomban P (1993) *J Mater Sci* 29:3705–3718. doi:[10.1007/bf00357338](https://doi.org/10.1007/bf00357338)
- [32] de Bonis C, Cozzi D, Mecheri B et al (2014) *Electrochim Acta* 147:418–425. doi:[10.1016/j.electacta.2014.09.135](https://doi.org/10.1016/j.electacta.2014.09.135)
- [33] Amirinejad M, Madaeni SS, Rafiee E, Amirinejad S (2011) *J Membr Sci* 377:89–98. doi:[10.1016/j.memsci.2011.04.014](https://doi.org/10.1016/j.memsci.2011.04.014)

- [34] Ramani V, Kunz HR, Fenton JM (2004) *J Membr Sci* 232:31–44. doi:[10.1016/j.memsci.2003.11.016](https://doi.org/10.1016/j.memsci.2003.11.016)
- [35] Ramani V, Kunz HR, Fenton JM (2005) *Electrochim Acta* 50:1181–1187. doi:[10.1016/j.electacta.2004.08.015](https://doi.org/10.1016/j.electacta.2004.08.015)
- [36] Lin C, Haolin T, Mu P (2012) *Int J Hydrog Energy* 37:4694–4698. doi:[10.1016/j.ijhydene.2011.04.116](https://doi.org/10.1016/j.ijhydene.2011.04.116)
- [37] Shang F, Li L, Zhang Y, Li H (2009) *J Mater Sci* 44:4383–4388. doi:[10.1007/s10853-009-3658-6](https://doi.org/10.1007/s10853-009-3658-6)
- [38] Wang J, Wasmus S, Savinell RF (1995) *J Electrochem Soc* 142:4218–4224. doi:[10.1149/1.2048487](https://doi.org/10.1149/1.2048487)
- [39] Mahreni A, Mohamad AB, Kadhum AAH, Daud WRW, Iyuke SE (2009) *J Membr Sci* 327:32–40. doi:[10.1016/j.memsci.2008.10.048](https://doi.org/10.1016/j.memsci.2008.10.048)